Growth-induced self-organization in bacterial colonies

You, Z.

Chapter 4

Confinement-induced self-organization

In chapter 3, we have seen that in freely expanding bacterial colonies, competition between the growth-induced active stress and the passive elastic forces originating from cell-cell steric repulsion dominates the dynamics of the system and gives rise to randomly oriented nematic domains as well as turbulent cellular flows. In contrast, when the monolayered colony is confined laterally, this wild, chaotic behavior is replaced by a disciplined and ordered arrangement: cells collectively align with the confinement wall and a laminar-like flow emerges as a consequence of cell growth. This has been observed in various experiments and computer simulations [38, 51, 55, 59, 60]. A beautiful experiment was performed by Volfson *et al.*, where non-motile, rod-shaped bacteria were grown in a straight microfluidic channel with an outlet on both ends (Fig. 1.3) [38]. Initially, a few cells are placed at random locations in the channel. As the cells grow and duplicate, various micro-colonies arise, in which local nematic order can be found, but the system is globally isotropic (Fig. 1.3A). Immediately after the colony fills the channel, a global nematic order is developed, where cells collectively align with the channel wall (Figs. 1.3C and 4.1A).

This global alignment of cells with the confinement walls has very important biological implications [51]. If cells are randomly oriented, cell elongation toward the wall will generate large mechanical stress, which can significantly reduce the fitness of the cells [51]. In the case of collective alignment with the wall, all cells are pushing their neighbors toward the outlets. By doing so, not only can the growth-induced stress be released efficiently, but also a strong outward flow of cells is generated from the collective pushing, allowing cells to efficiently escape from the trap, and reduce the crowdedness of the whole colony [51]. In addition, the strong anisotropy in the globally aligned state can lead to a dramatic reduction of its tortuosity and enhance the nutrient diffusion in the preferred direction,

thus facilitating the nutrient intake of cells in bulk of the colony [51].

In a long channel, however, this globally ordered state becomes unstable through a buckling transition, where disordered nematic domains are created at the center of the channel and the system becomes partially ordered (Figs. 4.1C and 4.1D) [38, 59, 60]. This buckling instability was found to be triggered by the growth-induced axial compression, and can be captured by an elegant theory where the colony is modeled as a continuum uniaxial elastic medium [59]. Computer simulations of proliferating rods also revealed more sophisticated dynamics during the buckling transition, and how the transition was mediated by the cell growth rate, the cell aspect ratio, and the sliding friction from the substrate [60].

Whereas the understanding of the transition from global alignment to partial order is well, the mechanism of the development of global nematic order in the initial stage is still not very conclusive, despite of the crucial influence it has on the fitness of the bacterial colony. Two theories have been proposed to explain this phenomenon. Volfson *et al.* found that the global alignment of cells appeared simutaneously with the growth-induced expansion flow toward the outlets [38]. In addition, the global orientation of cells coincides with the direction of the expansion flow, i.e., parallel to the chamber wall (Figs. 4.1A and 4.1B). Based on these findings, they conjectured that the global alignment was driven by the expansion flow. A phenomenological theory was developed based on the hydrodynamic equations of nematic liquid crystals, where the nematic order parameter S was coupled to the flow gradient, which, when nonzero, favored perfect nematic order, i.e. $S = 1$. This theory can qualitatively reproduce the results from the experiments and the simulations, but no reasoning was provided to justify the coupling between the flow and the nematic order parameter S, which was the core of the theory. Most recently, a stochastic theory was proposed to explain the global alignment [103]. The authors modeled cell growth in a rectangular microfluidic trap as a spatial Moran process, and concluded that the wall alignment could drive the whole colony to align with the long axis of the trap. However, these results were based on two premises–asymmetric cell growth and the specific spatial dependence of cell growth rate. Specifically, a cell tends to grow more toward the nearest boundary than the opposite direction (asymmetry), and the grow rate of a cell decreases with its distance to the boundary (spatial dependence). These assumptions, if realistic, are by no means indispensable, according to the previous experiments and simulations [38,

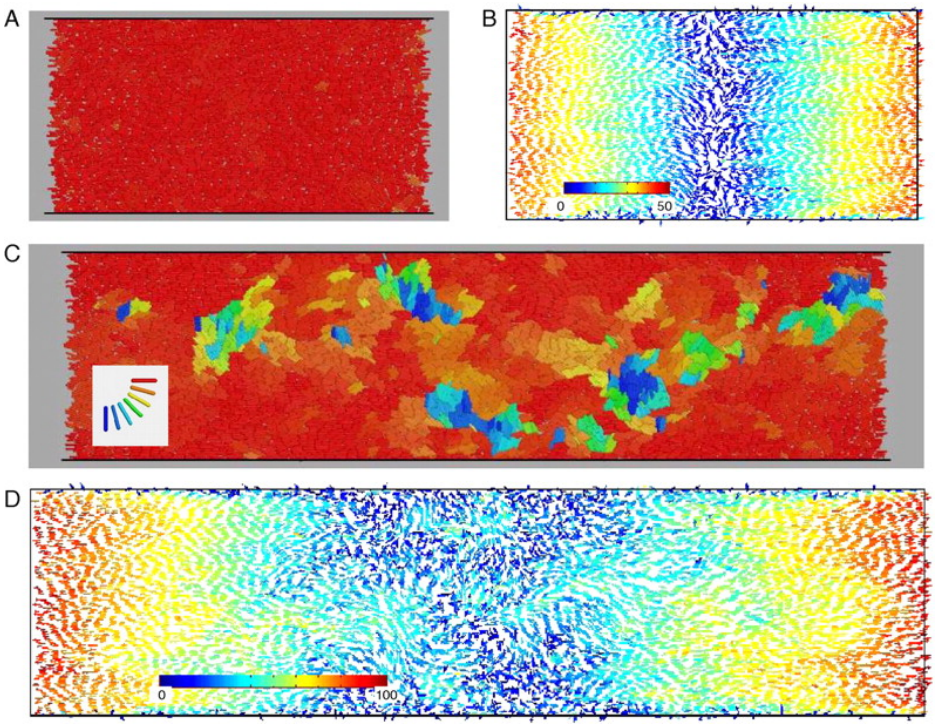

Figure 4.1. Discrete element simulations of the ordering dynamics in channels with different aspect ratios. (A) Orientation of individual cells (color-coded) in a short channel. (B) Velocity field for the same case as in A, where unit velocity vectors show the velocity direction for each cell and colors (from blue to red) correspond to the velocity magnitude (from low to high). (C) The same as A, but for a twice longer channel. Disordered nematic domains are constantly created in the middle of the channel and advected by the flow toward the open boundaries. (D) Velocity field for the long channel. The flow is no longer laminar, and there is no apparent correlation between orientation and velocity magnitude. Adapted from [38].

51, 55, 59, 60].

In this chapter, we demonstrate that the global alignment of cells is not triggered by either of these mechanisms, but instead is driven by the globally anisotropic stress emerging as a consequence of cell growth and confinement. Using computer simulations of the hard-rod model, we find that cell growth gives rise to a persistent accumulation of internal stress. While the stress components in the free direction can be efficiently released due to the expansion flow of cells toward the outlets, the presence of confinement prohibits cell motion in the confined direction, and leads to a build up of the corresponding stress components. As a consequence, a globally anisotropic stress emerges, where the stress components in the confined direction are larger than their orthogonal counterparts. This anisotropic stress can destabilize the vertical alignment (i.e. cells being vertical to the confinement walls), while making the horizontal alignment more stable and, therefore, drives cells to align with the direction of minimal stress which, in the case of a straight channel, is parallel to the wall. These discoveries not only shed new light on the roles of confinement and mechanical stress on the self-organization of growing bacterial colonies and more generally the interplay between orientation and stress in nematic liquid crystals, but also provide a potential way to control growing bacterial colonies with confinement.

4.1 Phenomena

We use the hard-rod model introduced in section 2.1 and constrain the colony in the xy–plane as we did in chapter 3. All control parameters in chapter 3 apply to this chapter as well: $d_0 = 1\,\mu$m, $Y_c = 4$ MPa, and $\zeta = 200$ Pa h. We confine the growing colony with a rectangular box of dimension $L_x \times L_y$, and centered at the origin $[0, 0]$. Specifically, two horizontal confinement boundaries of length L_x are placed at $[0, -L_y/2]$ and $[0, L_y/2]$, respectively. The horizontal boundaries can represent either impenetrable rigid walls, interacting stericly with the cells or, periodic boundaries, which make the system periodic in the y direction. Similar to the previous studies [38, 51, 55, 59, 60], we arrange two vertical absorbing boundaries at $[-L_x/2, 0]$ and $[L_x/2, 0]$, as the outlets of the channel. Cells overlapping with the absorbing boundaries will be removed from the system. This allows continuous growth of cells in the channel without overcrowding and jamming of cell motion. We call the extent of channel

in x, L_x, the width of the channel, and that in y, L_y, the channel height. In all snapshots shown in this chapter, we use solid white lines to represent the rigid walls, dashed white lines the periodic boundaries, and red solid lines the absorbing boundaries. All simulations start with a cell at the origin, with random orientation. In this chapter, we fix the cell growth rate at $g = 2\mu$m/h and the division length at $l_d = 2\mu$m, and focus on the effects of boundary condition and channel geometry on the colony dynamics. SI units are used in this chapter.

We first study growing bacterial colonies confined by rigid walls. Figures 4.2a–i show snapshots at typical stages of a growing colony under this confinement. As expected, a steady state of global nematic order is finally reached, where cells mostly align in the horizontal direction. An obvious conjecture is that the global alignment is driven by boundary anchoring,

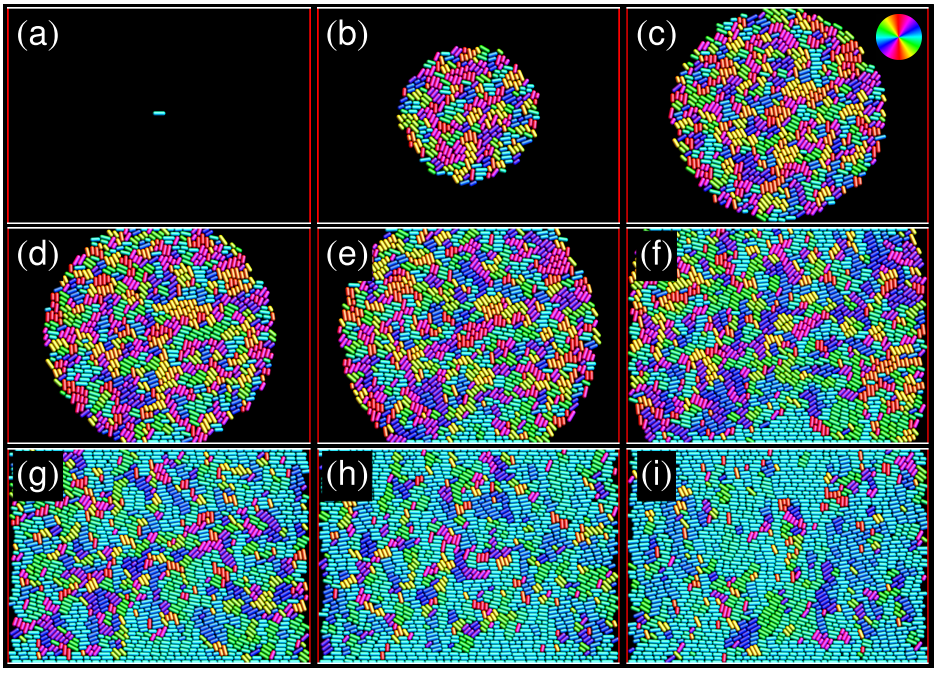

Figure 4.2. Snapshots at different time points of a growing colony subject to rigid wall confinement in the y direction. The horizontal white lines represent the rigid walls, and the vertical red lines the absorbing boundaries. Cells are color coded by their orientation, as indicated by the color wheel in (c). The simulation parameters are: $L_x = 70$ μm, $L_y = 50$ μm.

as proposed in Ref. [103]. Indeed, steric repulsion from the rigid walls can generate net torques on cells nearby, and enforce them to be parallel to the wall. This effect is usually referred to as *parallel boundary anchoring* in the theory of liquid crystal [76]. In addition, neighboring cells also tend to align with each other as we showed in chapter 3. The parallel anchoring can then propagate into the bulk of the colony, and enforce the whole colony to be aligned with the wall. This boundary driven alignment is commonly seen in nematic systems [76], and was also observed recently in cellular monolayers (Fig. 4.3) [102, 104].

Although simple and intuitive, this explanation turns out to be inadequate. As shown in Ref. [104], the boundary anchoring can only propagate toward the bulk up to a distance that is proportional to the orientation correlation length. Hence, the global alignment can only appear when

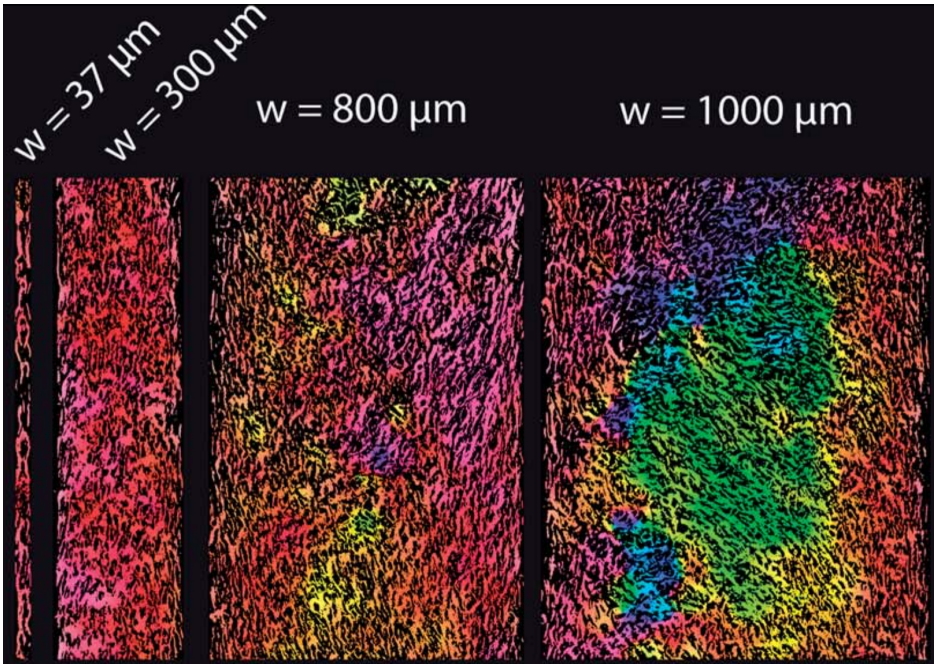

Figure 4.3. Orientation of the cells in stripes of different width at long times. Cells are color coded by their orientation as indicated by the legend on the right hand side. Note the homogeneous orientation at small widths and the patchy aspect at large widths that indicate the presence of well-oriented clusters with a different orientation. Adapted from [104].

the channel height L_y is smaller than this "penetration depth" (Fig. 4.3) [104]. For high channels, wall alignment can be expected within the penetration depth, but the rest of system is globally disordered (Fig. 4.3) [104]. In our case of growing bacterial colonies, as we discussed in chapter 3, the orientation correlation length is mediated by the competing effects of cell aspect ratio and the growth rate. For $l_d = 2$ μm and $g = 2$ μm/h, this correlation length is about a few cell widths (Figs. 4.2b and 4.2c). Indeed, in Figs. 4.2d–f, we do see the boundary alignment stops at a few cell widths from the walls. Therefore, the boundary anchoring by itself is not sufficient to induce horizontal alignment in the whole colony. To further demonstrate this point, we eliminate the boundary anchoring effect by replacing the rigid walls with periodic boundaries. This setup can represent cell growth on a cylindrical surface, provided the effects from the curvature can be ignored. As expected, even without boundary anchoring, the globally horizontal alignment still appears (Figs. 4.4a–i).

Let us now look at the development of the global alignment. Take the periodic case as an example. Initially, the colony can freely expand and is globally isotropic with no preferred orientation, as shown in Figs. 4.4b-d. When the top and the bottom fronts collide on each other, the confinement starts to take effects. At first, only the cells at the front (i.e. close to the periodic boundaries) reorient along the horizontal direction (Fig. 4.4e). Later, there are some disconnected domains in bulk of the colony aligning in the same direction (Fig. 4.4f). Then, these domains expand (Fig. 4.4g), merge (Fig. 4.4h), and finally, global alignment along the horizontal direction is extended to the whole colony (Figs. 4.4i). Similar process can be found in the case of rigid walls (Figs. 4.2a–i). An exception is that the boundary anchoring effect from the rigid walls can facilitate the global alignment to some extent. For this reason, the global alignment develops more rapidly and the steady states are more ordered in presence of rigid walls. From this perspective, the emergence of global alignment is more like a percolation process emerging from all over the colony than a propagation process initiated at the boundary [105]. These results suggest that the confinement of cell motion must have triggered some mechanical effects that can drive cells to align in the horizontal direction.

A strong candidate among the possible mechanical effects is the flow alignment of the nematic director. As demonstrated by Volfson *et al.*, the combined effects of confinement and cell growth give rise to an expansion flow of cells, which arises simutaneously with the global alignment, and

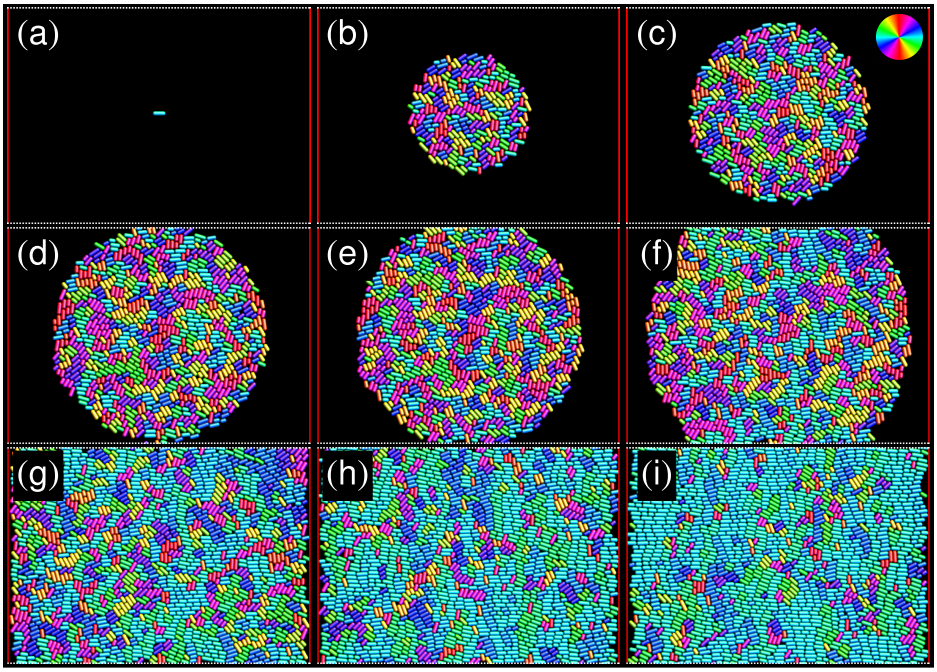

Figure 4.4. Snapshots at different time points of a growing colony subject to periodic confinement in the y direction, represented by the dashed white lines. Cells are color coded by their orientation, as indicated by the color wheel in (c). The simulation parameters are: $L_x = 70$ μm, $L_y = 50$ μm.

whose direction and gradient both coincide with the orientation of cells (Figs. 4.1A, 4.1B, and 4.5a) [38]. Although the specific flow–orientation coupling in their theory is different from the "standard" flow alignment in nematic liquid crystals, it is similar in spirit: flow velocity gradient can drive nematic order. To explain this, imagine a steady laminar flow $\boldsymbol{v} = v_x(x)\hat{\boldsymbol{x}}$ in the channel, with a constant flow gradient in x: $\partial_x v_x = C > 0$. In such case, the vorticity tensor $\boldsymbol{\omega}$ vanishes, and Eq. 2.4c can be simplified as

$$\frac{DQ_{xx}}{Dt} = \lambda SC + \gamma^{-1} H_{xx}, \tag{4.1a}$$

$$\frac{DQ_{xy}}{Dt} = \gamma^{-1} H_{xy}. \tag{4.1b}$$

Equations 4.1 indicate the tendency of nematic director to align with the flow gradient. Specifically, the term λSC provides a positive feed to

$Q_{xx} \equiv S(n_x^2 - 1/2)$ and tends to increases it, while there's no such term for $Q_{xy} \equiv S n_x n_y$. Overall, this can drive Q_{xx} toward the maximum value of $1/2$, corresponding to a perfect nematic order $S = 1$, with a horizontally aligned director $\boldsymbol{n} = \hat{\boldsymbol{x}}$.

To characterize quantitatively the relations between the flow and the cell orientation, we define an *alignment parameter* of cell orientation

$$\Phi = 2\left[\left\langle p_x^2 \right\rangle - \frac{1}{2}\right], \tag{4.2}$$

where $\boldsymbol{p} = [p_x, p_y]$ is the orientation of each cell and $\langle\cdot\rangle$ represents an average over all cells in the region concerned. Defined in this way, Φ quantifies the degree of alignment of cells with the x-axis: $\Phi = 1$ when all cells are parallel to $\hat{\boldsymbol{x}}$; $\Phi = 0$ when they are randomly oriented; $\Phi = -1$ if they all parallel to $\hat{\boldsymbol{y}}$. Similarly, the alignment parameter of flow can be defined as

$$\Phi_v = 2\left[\left\langle (v_x/|\boldsymbol{v}|)^2 \right\rangle - \frac{1}{2}\right], \tag{4.3}$$

which again, quantifies the alignment of flow with the x-axis in the same way. Figures 4.5c–e show the time evolution of Φ, Φ_v, and the flow gradient $\partial_x v_x$, in a periodically confined colony as well as a freely expanding one. We focus on different regions in the two colonies. In the confined colony, we are interested in the region where the confinement takes effects. We call it region I, and define it as $|x| < D_x/2 - 15$ μm, where D_x is the horizontal extension of the colony and 15 μm the approximate width of the two "unconfined" caps on both sides of the colony (Fig. 4.5a). We denote t_c as the time at which the confinement starts to take effects. Before the colony is confined, i.e., $t < t_c$, cells in region I have no preferential orientation (Fig. 4.5c), and the flow mostly aligns with the y-axis (Fig. 4.5d). After t_c, a rapid reorientation of the flow toward x can be found, accompanied with an amplification of the flow gradient along x (Fig. 4.5e). At the same time, we can see a gradual increase of alignment parameter Φ. These results suggest that the flow alignment might be the dominant mechanism of the global cell alignment. However, comparison with the freely expanding colony demonstrates that it's just a fortuitous coincidence. In a freely expanding colony, because of the rotational symmetry, both flow and its gradient are radial (Fig. 4.5b). This means that if we consider only a narrow sector of the colony, region II for example (defined as $|y| < 5$ μm), the flow field will be similar to that of region I

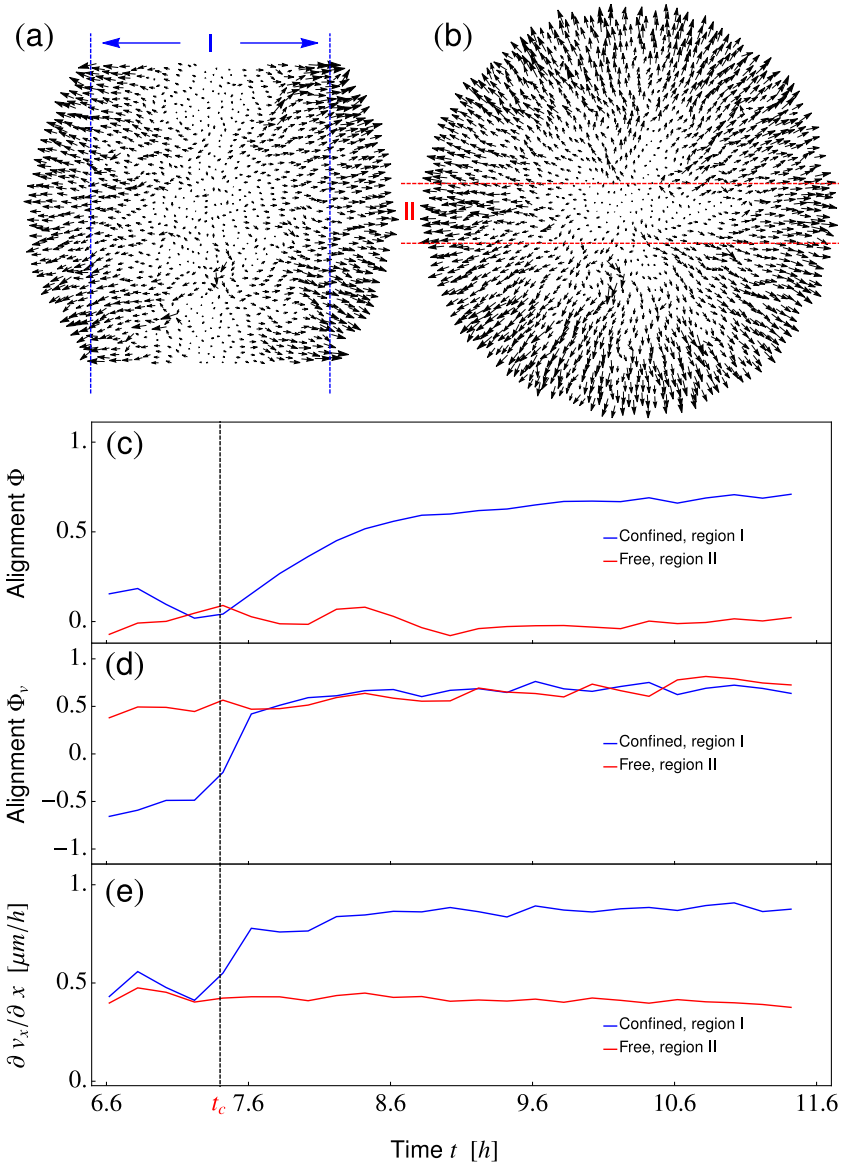

Figure 4.5. (a–b) Flow fields of (a) a periodically confined colony (i.e. the colony shown in Figs. 4.4) and (b) a free colony. Each arrow represents the velocity of the corresponding cell, with an arrow length proportional to the cell speed. (c–e) (c) The orientation alignment parameters, (d) velocity alignment parameters, and (e) the flow gradient, in confined (blue lines) and free (red) colonies. The dashed indicates the time t_c, at which the confinement starts to take effects.

in a confined colony. Indeed, Fig. 4.5d shows the same degree of horizontal alignment of flows in the two regions for $t > t_c$, except that the flow gradient is smaller in the free colony (Fig. 4.5e). If the flow alignment indeed dominates, we would expect cells in region II of the free colony to align horizontally as well, which however, is never found, hence disproves the flow alignment mechanism.

4.2 Stress anisotropy drives cell alignment

In this section, we propose a new mechanism for this global alignment– stress anisotropy drives cell reorientation. As shown in chapter 3, cell growth can increase the local packing fraction, and subsequently the local mechanical stress. In a freely expanding colony, the internal stress is released isotropically by the radial expansion flow (see e.g. Fig. 4.5b) and, consequently, can be decomposed into an isotropic pressure and an extensile active stress, both increasing linearly with the local packing fraction ϕ. We shall see now that the presence of confinement completely changes the growth-induced stress and endows a new role to it.

To reveal the mechanical effects of confinement, we first study the time evolution of internal stress in a confined colony. The stress is measured in the same way as we did in chapter 3, but is expressed in the basis of $\hat{\boldsymbol{x}}$

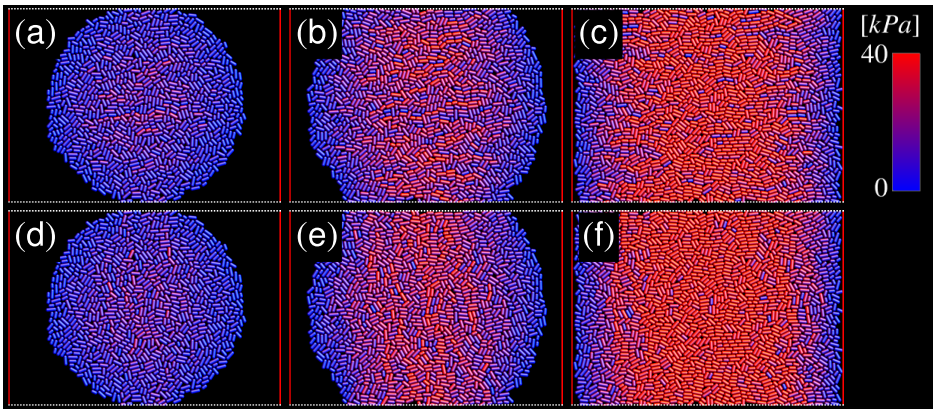

Figure 4.6. Snapshots of the periodically confined colony (i.e. colony shown in Figs. 4.4) at different time points. Cells are color coded by the mechanical stresses they experience: (a-c) $|\sigma_{xx}|$ and (d-f) $|\sigma_{yy}|$. The color map is shown in the legend on the right hand side.

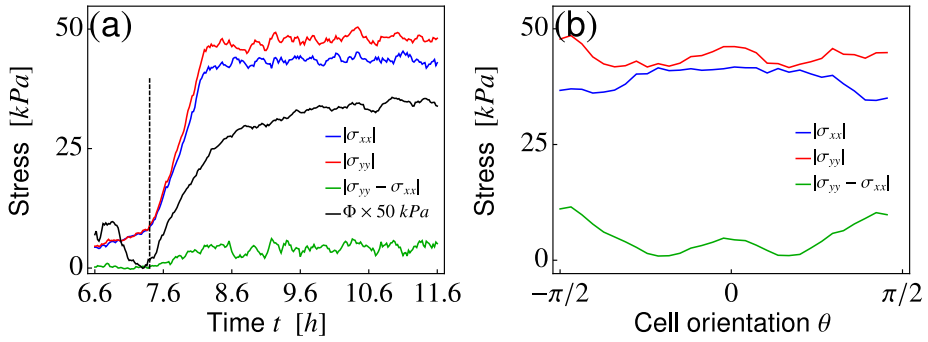

Figure 4.7. (a) Development of the average stresses and the alignment parameter in region I of the periodically confined colony. The black dashed line indicates t_c, the time at which the confinement starts to take effects. Here, we times Φ by 50 kPa in order to directly compare its trend with those of the stresses. (b) Dependence of stress components in region I on the cell orientation θ.

and $\hat{\boldsymbol{y}}$:

$$\boldsymbol{\sigma} = \sigma_{xx}\hat{\boldsymbol{x}}\hat{\boldsymbol{x}} + \sigma_{yy}\hat{\boldsymbol{y}}\hat{\boldsymbol{y}} + \sigma_{xy}(\hat{\boldsymbol{x}}\hat{\boldsymbol{y}} + \hat{\boldsymbol{y}}\hat{\boldsymbol{x}}). \tag{4.4}$$

Similar to the previous chapter, we ignore the shear component σ_{xy} and focus only on the normal components σ_{xx} and σ_{yy}. Figures 4.6a–f show the two normal stresses that each cell experiences at different time points. Upon confinement, both stresses increase dramatically.

To quantify the effects of confinement on the stress, we focus on the average stress of cells in the "confined region", i.e. region I in Fig. 4.5a. As shown in Fig. 4.7a, for $t > t_c$, both stress components increase, but $|\sigma_{yy}|$ on average is larger than $|\sigma_{xx}|$, indicating that the stress is globally anisotropic. This stress anisotropy originates from the combined effects of cell growth and boundary confinement. On the one hand, cell growth provides a persistent feed to the internal stresses. On the other hand, the absence of cell motion in the confined direction prevents the normal stress in y, σ_{yy}, to be released, while the normal stress in x, σ_{xx}, can still be released efficiently. Consequently, $|\sigma_{yy}| > |\sigma_{xx}|$ in the confined region. In addition, the normal stress difference $|\sigma_{yy} - \sigma_{xx}|$ also depends on the cell orientation: $|\sigma_{yy}| > |\sigma_{xx}|$ is valid for all cell orientations, and is maximized at $|\theta| \approx \pi/2$, i.e. for vertically aligned cells (Fig. 4.7b). The orientational dependence of stress components can also be observed in Figs. 4.6b and 4.6e, where larger σ_{xx} and σ_{yy} appear more frequently to horizontal and vertical cells, respectively. This is because the anisotropic cell growth

gives a stress feed of the extensile form $\alpha(\boldsymbol{nn} - 1/2)$, contributing more to the stress components parallel to the cell axis than those in the orthogonal direction. Especially, the growth of vertical cells in the confined region can rapidly increase σ_{yy}, as well as the normal stress difference.

The globally anisotropic stress can be rearranged into an isotropic pressure and a net compression in the y direction:

$$\begin{aligned} \boldsymbol{\sigma} =& \sigma_{xx}\hat{\boldsymbol{x}}\hat{\boldsymbol{x}} + \sigma_{yy}\hat{\boldsymbol{y}}\hat{\boldsymbol{y}} \\ =& \sigma_{xx}\boldsymbol{I} + \beta\hat{\boldsymbol{y}}\hat{\boldsymbol{y}}, \end{aligned} \tag{4.5}$$

where $\beta = (\sigma_{yy} - \sigma_{xx})$ is the magnitude of the net compression. Cell orientation is not directly influenced by the isotropic pressure, but can be regulated by the net compression $\beta\hat{\boldsymbol{y}}\hat{\boldsymbol{y}}$. For vertically aligned cells, the net compression is parallel to the nematic director and, as demonstrated in chapter 3, can bend the director and create a distortion, therefore destabilize the vertical alignment. This effect is further amplified by the fact that vertical cells experience the strongest net compression. On the contrary, the net compression can make the horizontal alignment more stable, because any deviation can induce a large restoring torque to bring the system back to balance. Furthermore, as cells grow and duplicate, the horizontally aligned domains, being more stable, can rapidly expand and cover larger portions of the colony area, which is consistent with what we've found before (Figs. 4.4e–g). Altogether, this specially structured anisotropic stress can drive cells to align horizontally, and we conjecture that it is the dominant mechanism for the global alignment of cells.

To demonstrate that the stress anisotropy is sufficient to drive the global alignment, and gain further insight into the interplay between stress and cell orientation, we perform a simulation of shrinking box. Specifically, we manually arrange a collection of non-growing cells of identical length $l = 2\mu$m in a box that is periodic in both x and y, so no boundary anchoring in such setup. Initially, each cell has a random position and a random orientation. Then we gradually shrink the box in the y direction in order to create a stress anisotropy (Figs. 4.8a–c). This is done by rescaling the y-coordinates of all cells as well as those of the horizontal boundaries by $y(t + \Delta t) = k'y(t)$, where $k' = (L_y - V_y\Delta t)/L_y$ is the rescaling factor and V_y the relative speed of the two horizontal boundaries. Since all y-coordinates are rescaled by the same factor at each time step, the vertical shrinking is homogeneous over the whole system. Note that p_y, the y-th component of the cell orientation, is not rescaled during this process.

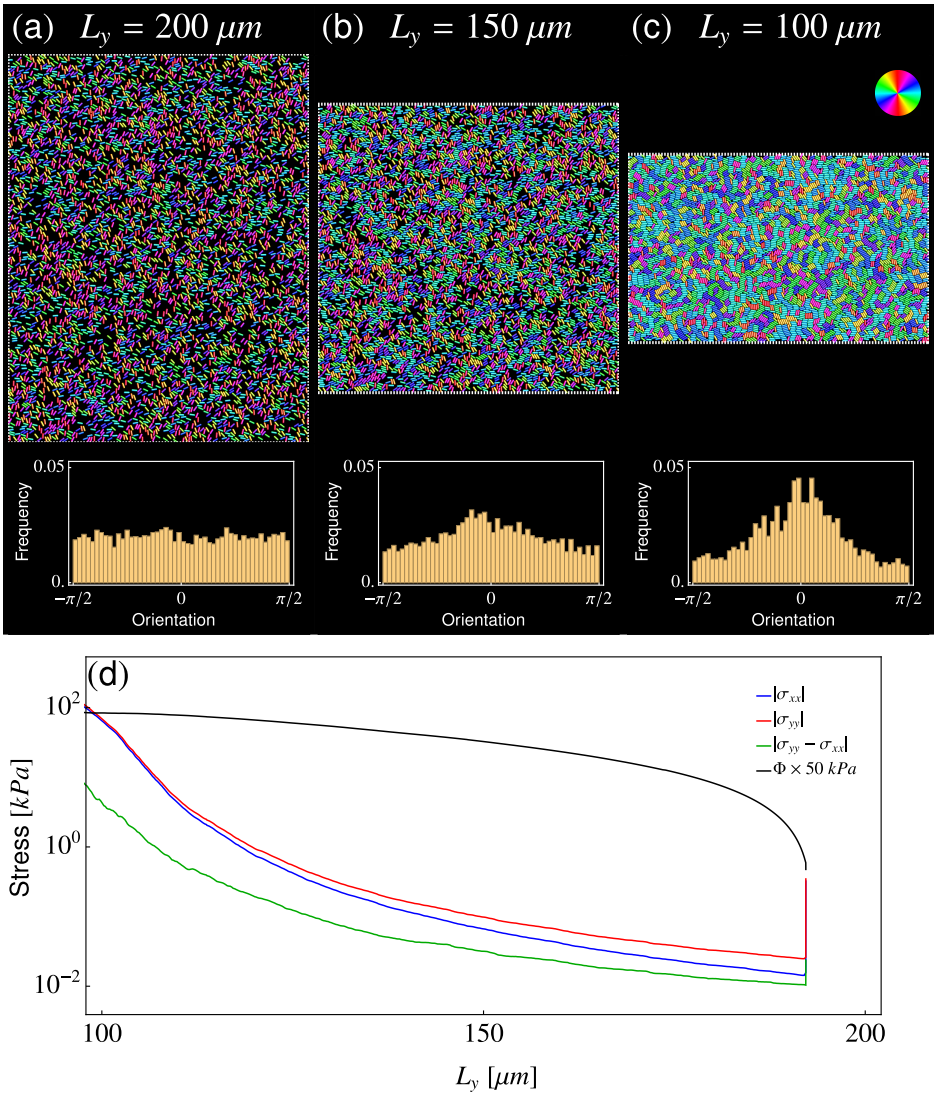

Figure 4.8. Dynamics of the shrinking colony. (a–c) Snapshots at different time points. Cells are color coded by their orientations according to the color wheel in panel (c). The insets show the histograms of the cell orientation at the corresponding time points. The system is periodic in both x and y. The system contains 5000 cells in total, with a width $L_x = 150$ μm and an initial height $L_y = 200$ μm. The shrinking speed, i.e. the relative speed between the top and the bottom boundaries, is $V_y = 10$ μm/h. (d) The average stresses and the global alignment parameter Φ as functions of the box height L_y. Again, we times Φ by 50 kPa in order to directly compare the trends of Φ and the stress components.

Figures 4.8a–d summarize the dynamics of the shrinking colony. The system is initially isotropic, orientationally (Fig. 4.8a) and mechanically (right side of Fig. 4.8d), represented by the uniformly distributed cell orientation and the small alignment parameter Φ. Once the shrinking is applied, σ_{yy} increases and, quite surprisingly, same as σ_{xx}, but the former increases faster. There are two reason to account for the increase of σ_{xx}. First, increasing the cell-cell overlap distance in y (when shrinking) may also increase the x component of the repulsive forces between neighboring cells. Second, the emerging anisotropic stress, as a consequence of anisotropic shrinking, can drive cells to reorient toward the horizontal direction (Fig. 4.8b and its inset) which, in turn redistributes the stress by decreasing σ_{yy} and increasing σ_{xx}, therefore diminishes the stress anisotropy. From this perspective, the reorientation of cells toward the direction of minimal stress is a strategy for the system to minimize the total elastic energy by redistributing the two normal components. For this reason, σ_{yy} does not deviate significantly from σ_{xx} (Fig. 4.8d), because further deviation can cause an additional reorientation of cells, which in turn reduces the stress anisotropy. In growing bacterial colonies, this negative feedback on stress anisotropy from cell reorientation is even more profound because the reorientation of cells not only directly redistributes the normal stresses, but also changes the growth-induced stress feed $\alpha(\boldsymbol{nn} - 1/2)$, which can further reduce the normal stress difference. Consequently, the normal stress difference is always much smaller than the two normal stresses (Figs. 4.7a and 4.7b). As the system shrinks further, both normal stresses as well as their difference increase, driving more and more cells to align in x and, finally, a highly aligned state is reached, where cell orientation is peaked at $\theta = 0$ (Fig. 4.8c and its inset). These results not only confirm that the stress anisotropy can indeed drive horizontal alignment, but also demonstrate a mutual regulation between cell orientation and the mechanical stresses.

We will now go back to the growing colony, and find the relation between cell orientation and the stress anisotropy to support our theory. The simplest evidence is to compare the time evolution of the two quantities. As shown in Fig. 4.7a, the alignment parameter Φ indeed increases simutaneously with the normal stress difference $|\sigma_{yy} - \sigma_{xx}|$. However, these quantities are averaged over the whole region I and, therefore, do not contain any information about the spatial variations of the stresses. Furthermore, in colonies subject to periodic or rigid wall confinements, during

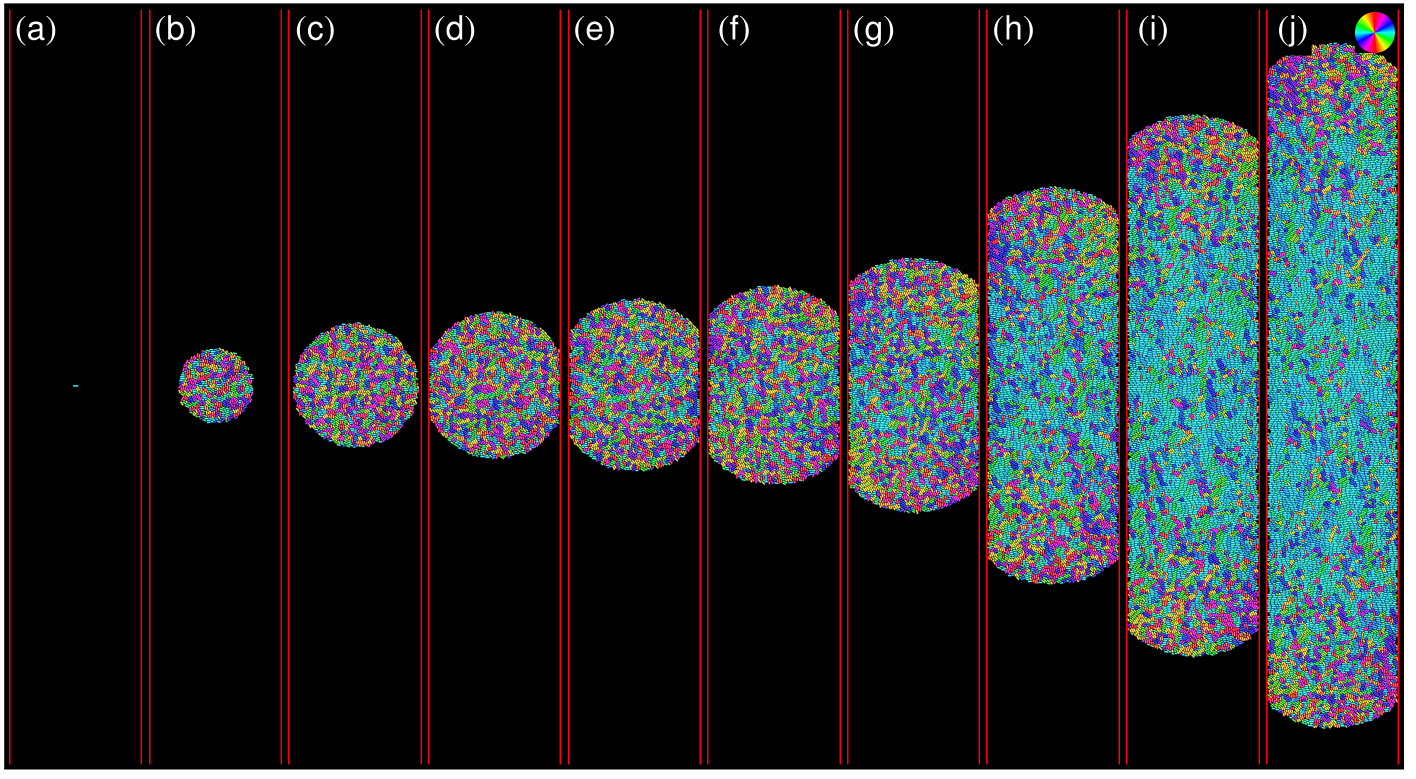

Figure 4.9. Snapshots of the growing colony that can freely expand in the vertical direction, at different time points. Cells are color coded by their orientation, as indicated by the color wheel in panel (j). The channel width is $L_x = 70$ μm, and the heights of all panels are 300 μm.

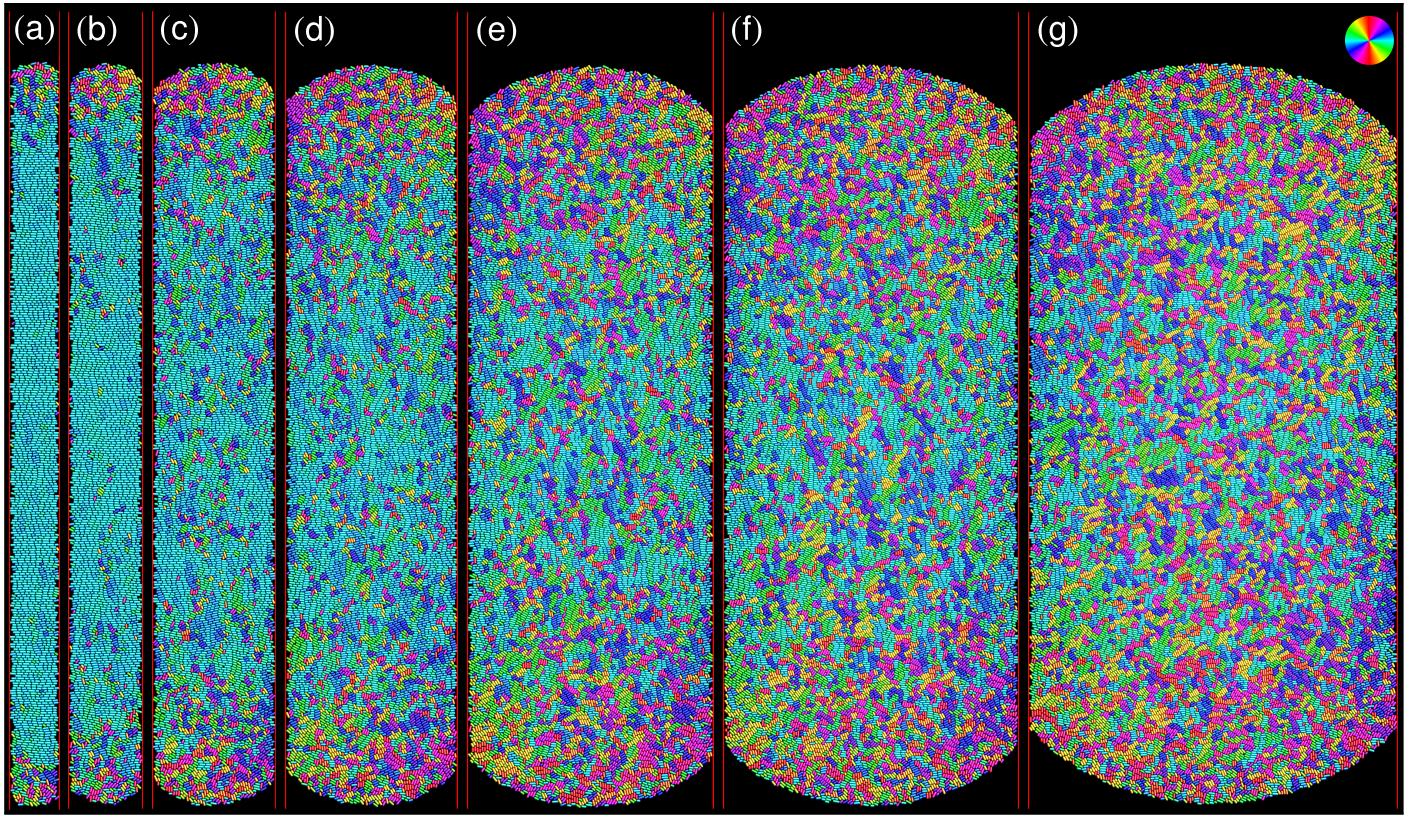

Figure 4.10. Snapshots of the unconfined colony with different L_x values: (a) 20 μm, (b) 40 μm, (c) 50 μm, (d) 70 μm, (e) 100 μm, (f) 120 μm, (g) 150 μm. The heights of all panels are 300μm. Cells are colored coded by their orientations, as indicated by the color wheel in panel (g).

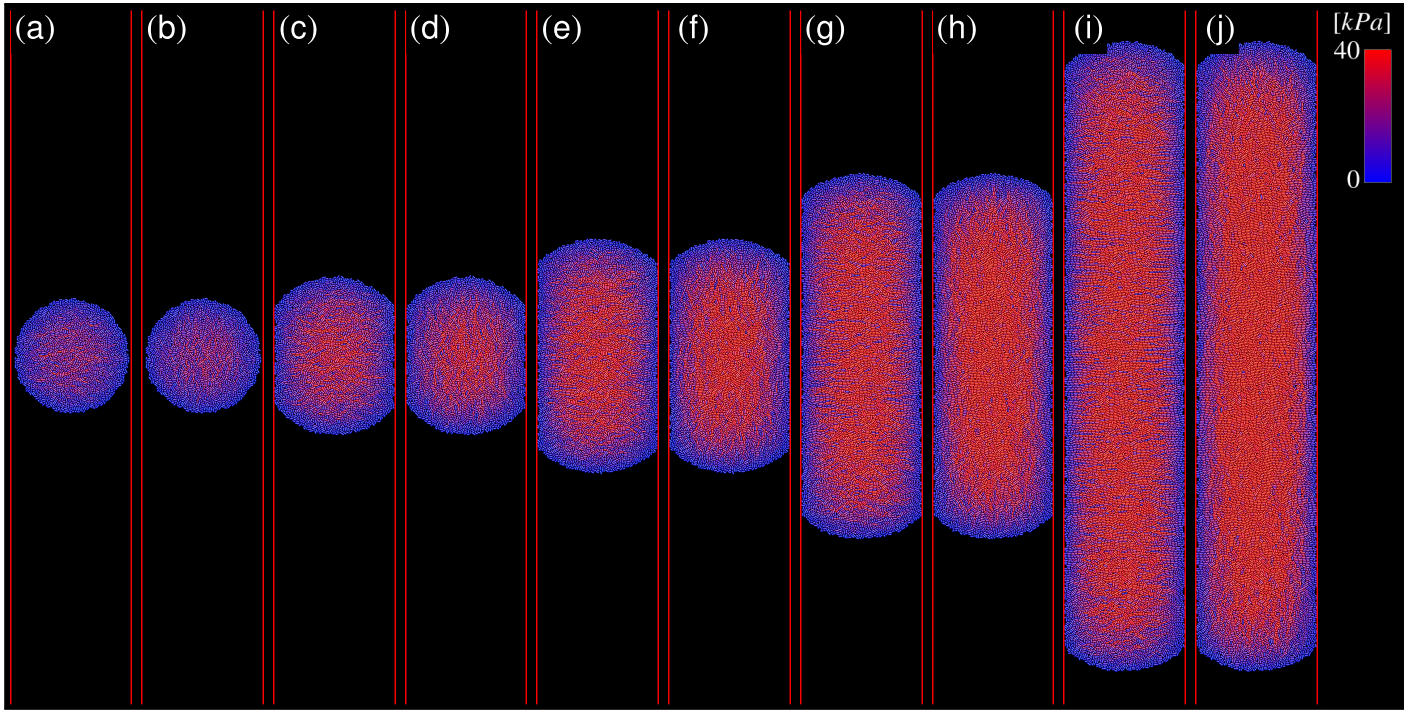

Figure 4.11. Stress distributions of the colony shown in Figs. 4.9 at different time points. Cells are color coded by the mechanical stresses they experience: (a, c, e, g, i) $|\sigma_{xx}|$ and (b, d, f, h, j) $|\sigma_{yy}|$. The color map is shown in the legend on the right hand side.

the development of global alignment, the system shows strong spatial and temporal inhomogeneities. Specifically, the stress has a large spatial variation, which is also rapidly evolving in time. It is very difficult to collect adequate samples to faifthfully capture the subtle interplay between stress and cell orientation. For this reason, we change the simulation setup by removing the vertical confinement and allow the colony to freely expand in the vertical direction. Surprisingly, even without an explicit confinement, the global alignment still appears, but at a much slower pace. Specifically, after an initial isotropic stage (Figs. 4.9a–e), a horizontal alignment gradually emerges from the horizontal axis of the colony, i.e. at $y = 0$ μm (Fig. 4.9f), when the colony's extension in y, denoted by R_y for convenience, becomes reasonably larger than that in x. As the colony explores further in y, the horizontally aligned region expands at a constant speed, leaving two disordered caps, of constant heights, symmetrically placed on the two ends of the elongated colony (Figs. 4.9g–j). More interestingly, increasing the channel width L_x makes it more difficult to develop the horizontal alignment and results in larger disordered caps (Figs. 4.10a–g).

These phenomena, again, can be ascribed to the anisotropic stress arising during the colony expansion. Figures 4.11a–j show the normal stresses that each cell experiences at different time points in the unconfined colony. Both $|\sigma_{xx}|$ and $|\sigma_{yy}|$ increase with time and decrease from the colony center to the vertical or horizontal boundaries as expected. For simplicity, we focus on the region $|x| < 10$ μm, and call it region III for convenience. The spatial distributions of stresses and alignment parameter Φ in region III are shown in Figs. 4.12a–e. Due to the elongated shape of the colony, in order to grow, cells in the bulk need to push more cells away in the vertical direction than in the horizontal direction. An anisotropic stress hence arises where $|\sigma_{yy}| > |\sigma_{xx}|$, and this stress anisotropy decreases monotonically with $|y|$, the vertical distance from the colony center (Figs. 4.12b–c). As the colony morphology becomes more anisotropic, the region with anisotropic stress expands, and the normal stress difference at a given location also increases with time (Fig. 4.12d). This explains why the horizontal alignment appears first at $y = 0$ μm, and then gradually expands in the vertical direction. Finally, most cells in the colony bulk align well in the horizontal direction (Fig. 4.9j). Without stress feed in y, and with a steady release of σ_{xx} by the expansion flow, both normal stresses as well as their difference saturate at certain values, and the colony bulk reaches a steady state (Fig. 4.12e). In wider channels, σ_{xx} at given

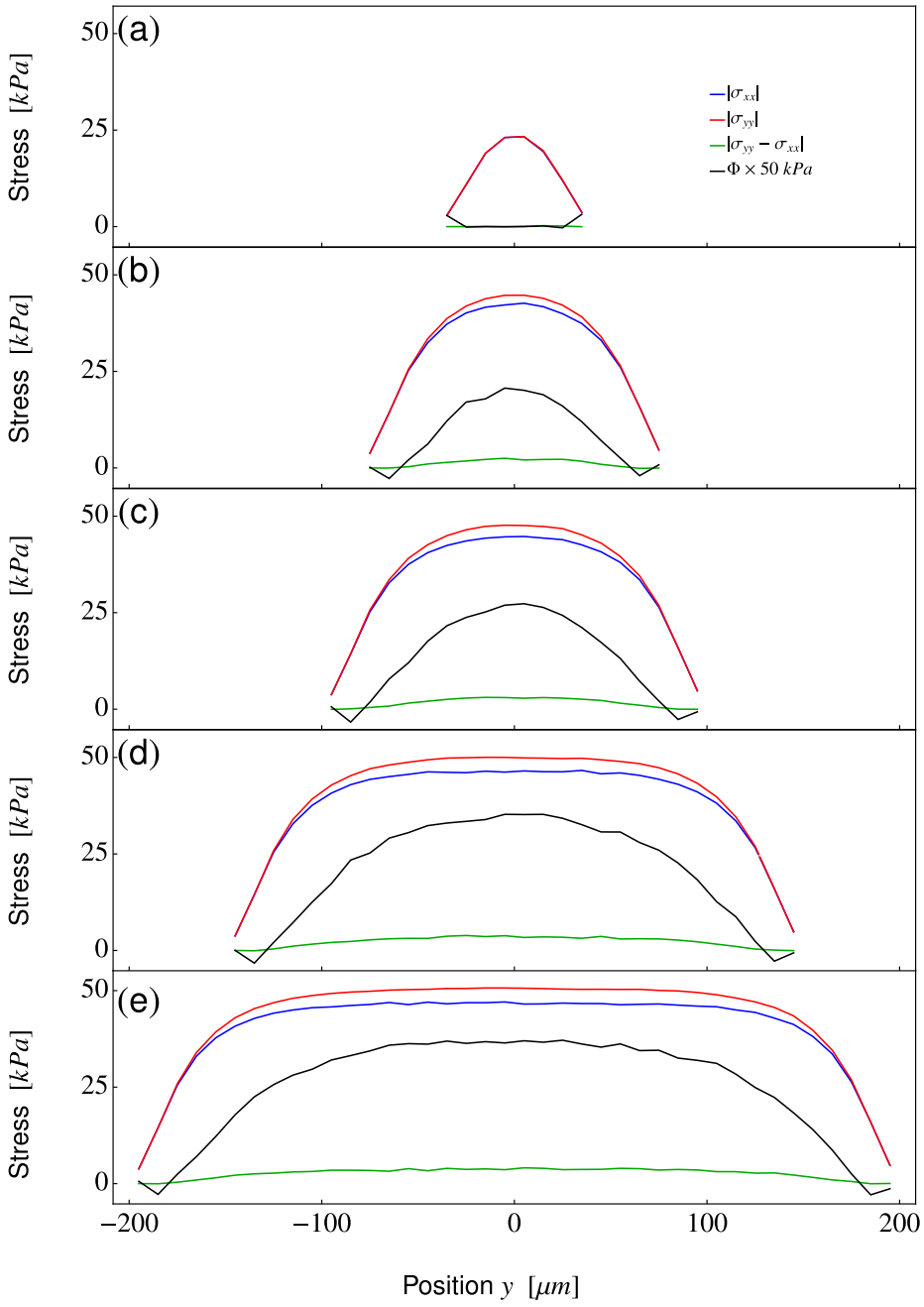

Figure 4.12. Spatial distributions of stresses and Φ in region III of an unconfined colony at different time points. The colony extensions in y, R_y's, are: (a) 70 μm, (b) 150 μm, (c) 190 μm, (d) 290 μm, and (e) 390 μm.

position, on average, is larger, hence requires larger R_y in order to create a stress anisotropy. Nevertheless, the horizontal alignment always emerges once the normal stress difference becomes nonzero.

These results suggest that the spatial-temporal variations of stresses and cell orientation are smoother in the unconfined colonies than the explicitly confined colonies, e.g. those shown in Figs. 4.2 and 4.4. In addition, one can easily control σ_{xx} and σ_{yy} in the unconfined colony by looking at different positions and different times, or changing the channel width L_x. Therefore, it is a perfect platform for us to study the relations between the horizontal alignment and the stress anisotropy. We notice that the expansion flow in bulk of the colony is mostly horizontal, and from $x = 0$ μm toward the outlets (i.e. $x = \pm L_x/2$). Hence, the local mechanical and orientational states of cells at the same height are correlated by the flow, while those at different heights are independent of each other. For this reason, we focus only on region III (i.e. $|x| < 10$ μm), the source of the expansion flow, and study the stresses and cell orientation at different heights and different time points of this region. To get as much data sample as possible, we grow the colony from a single cell until $R_y = 400$ μm, during which we take a sample snapshot whenever R_y increases by 10 μm. In each sample snapshot, we divide region III into small boxes, of dimension 20 μm$\times$10 μm, and then measure the average σ_{xx} and σ_{yy} over all cells in each box, as well as their alignment parameter Φ. We assume snapshots at different time points to be independent of each other. To explore further the parameter space, we change the channel width L_x from 50 μm to 150 μm with a step of 10 μm, and for each L_x we run 100 parallel simulations. These will give us a huge collection of sample boxes, each gives a specific combination of σ_{xx}, σ_{yy}, and alignment parameter Φ.

Figure 4.13a shows the phase diagram of the unconfined colony, spanned by the two normal stresses and the color indicates the average alignment parameter. The first thing to notice is that the system only occupies a very small region in the phase space: both normal stresses distribute closely to the line $|\sigma_{xx}| = |\sigma_{yy}|$ (white dashed line) in the phase space, due to the stress regulation by cell reorientation. In addition, there are more regions in the colony where $|\sigma_{yy}| > |\sigma_{xx}|$ because of the anisotropic colony morphology. Most importantly, horizontal alignment with large Φ (indicated as red), is more likely to be found in regions of large stress anisotropy. This is even more obvious in Fig. 4.13b, where the alignment parameter Φ increases monotonically with the stress anisotropy, defined

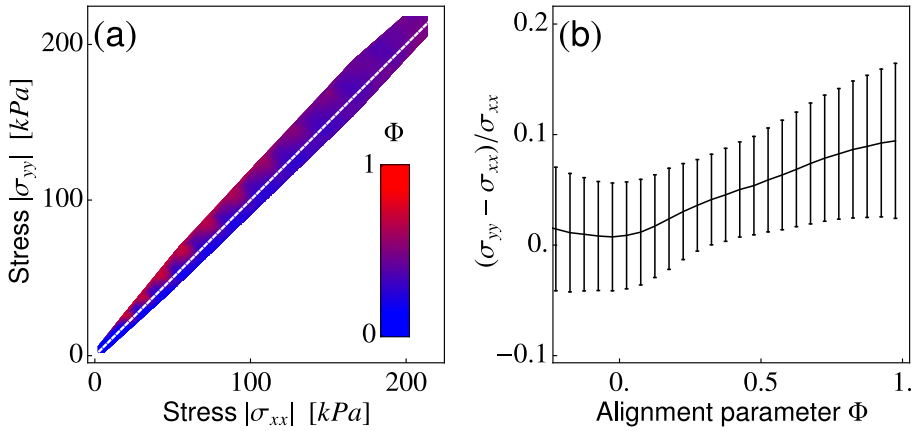

Figure 4.13. Statistical relations between the stress components and the alignment parameter in unconfined colonies. (a) Phase diagram of the unconfined colony, spanned by the two normal stresses and the color indicates the average alignment parameter. The color map is shown in the legend. The white dashed line indicates $|\sigma_{xx}| = |\sigma_{yy}|$. (b) Stress anisotropy, defined by $(\sigma_{yy} - \sigma_{xx})/\sigma_{xx}$, versus the alignment parameter. The error bars show the standard deviations of data samples about the average values.

by $(\sigma_{yy} - \sigma_{xx})/\sigma_{xx}$. At fixed Φ, though, the fluctuation of the stress anisotropy is quite large. This is because the two normal components have very similar values, so any small fluctuation of them can cause a dramatic change of the stress anisotropy. These results not only confirm our conjecture on the mechanism of horizontal alignment, but also validate our theory on the interplay between mechanical stresses and cell orientation.

4.3 Discussion and conclusion

In this chapter, we have explored the fascinating interplay among cell orientation, cell growth, and the mechanical stresses that cells experience. Cell orientation determines the direction of cell growth, and subsequently the growth-induced stress feed. The internal stress, if anisotropic, can drive cells to align with the direction of minimal stress. The reorientation of cells, in turn, not only redistributes the stress components, but also changes the direction of cell growth and accordingly the growth-induced stress feed. Both effects can reduce the normal stress difference and pro-

vide a negative feedback to the stress anisotropy. This three-way regulation loop not only dominates the dynamics of growing bacterial colonies, but also shapes them as smart materials that can actively regulate the internal stresses and navigate cell growth to maximize their fitness. An excellent example is, as shown in this chapter, the ability to deal with confinements during the colony expansion. The presence of confinement gives rise to a globally anisotropic stress, driving the cells to align in the unconfined direction and, guides the colony to expand in the easy direction.

In addition to the understanding of global alignment this theory provides, it also has some broader applications. In natural or artificial environments, bacterial colonies are frequently subject to different kinds of physical or geometrical confinements. This theory can predict cell orientation in such situations. For example, a phenomenon frequently observed in experiments is the merging of multiple colonies (Figs. 4.14a–d). In the merging region (highlighted by the colored boxes), cells collectively align with the common tangent of the two merging colonies. This is because the bulks of the two colonies act as confinements to cells at the merging fronts. Hence, cells reorient towards the common tangent and the merged colony expands much faster in the unconfined direction (Fig. 4.14c). Another example is cell growth on an elongated cylinder surface. Since cell motion is confined in the transverse direction, we can expect cells to align with the long axis of the cylinder. In addition, this theory also provides a potential way to control growing bacterial colonies with specifically engineered anisotropic stress. This can be done by applying confinements to the colony or, depleting cells at specific locations to drain the growth-induced stress. Also, as mentioned before, the internal stresses in the unconfined colony (see e.g. Fig. 4.9) follow very nice spatial patterns, which can be controlled by the channel width L_x or the colony extension R_y. This provides a nice setup to study the responses of cells to mechanical stresses.

Moreover, this theory also provides new insights into the physics of passive and active nematic liquid crystals. Increasing the packing fraction of lyotropic nematics, according to the classical Onsager theory, can cause a spontaneous symmetric breaking and drive the isotropic–nematic transition [76]. The resulting nematic phase, however, has no preferred orientation. Our theory, on the other hands, shows that the resulting global orientation can be decided beforehand, if the packing fraction is

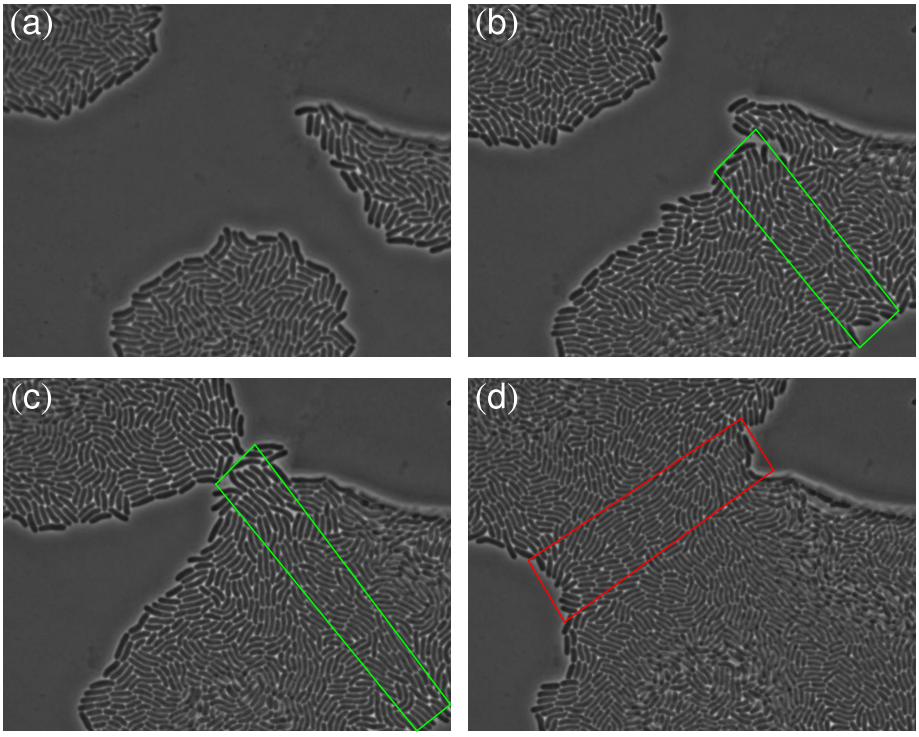

Figure 4.14. Experimental snapshots of the merging of three bacterial colonies at different time points. In the merging regions, i.e. those marked with colored boxes, cells collectively align with the common tangents of the two merging colonies. Images provided by Anupam Sengupta.

increased by applying anisotropic compression to the system. This is also in stark contrast with a recent study, which concluded that for moderately elongated spherocylinders, there was no orientational ordering upon athermal compression [106]. In addition, it has been extensively shown, experimentally and theoretically, that active matter systems, upon confinement, display a transition from chaotic dynamics to an ordered state [64, 86, 104, 107–109]. However, these results require the confinement to reduce the system size such that it's comparable to the system coherent length. Otherwise, the system will still be chaotic. Here, we show that in growing bacterial colonies, no such strong confinement is needed. The system can develop global order as long as the confinement leads to a global anisotropic stress. This introduces new roles of confinement to the

dynamics of active matter.

To look into the future, there are still unresolved problems along this line. For example, it is interesting to test our theory at different geometries, such as the microfluidic channels used in Ref. [51]. More quantitative characterization of the interplay between stress and cell orientation can definitely deepen our understanding on the mechanics of nematic liquid crystals. Finally, a continuum theory incorporating the coupling among mechanical stresses, cell orientation, and the cell growth, would be very useful for practical applications and theoretical studies.